Nanoscale Advances

ROYAL SOCIETY OF CHEMISTRY

PAPER

View Article Online
View Journal | View Issue

Cite this: *Nanoscale Adv.*, 2021, **3**, 2547

Surface modification for improving the photoredox activity of $CsPbBr_3$ nanocrystals†

Syed Akhil, V. G. Vasavi Dutt and Nimai Mishra *

Received 4th February 2021
Accepted 26th February 2021

DOI: 10.1039/d1na00091h

rsc.li/nanoscale-advances

In recent years inorganic lead halide perovskite nanocrystals (PNCs) have been used in photocatalytic reactions. The surface chemistry of the PNCs can play an important role in the excited state interactions and efficient charge transfer with redox molecules. In this work, we explore the impact of $CsPbBr_3$ nanocrystal surface modification on the excited state interactions with the electron acceptor benzoquinone (BQ) for three different ligand environments: as oleic acid/oleylamine (OA/OAm), oleic acid (OA)/trioctylphosphine (TOP), and oleic acid (OA)/oleylamine (OAm)/trioctylphosphine (TOP) ligands. Our finding concludes that amine-free PNCs (OA/TOP capped) exhibit the best excited state interactions with benzoquinone compared to the conventional oleylamine ligand environment. The photoinduced electron transfer (PET) rate constants were measured from PL-lifetime decay measurement. The amine-free PNCs show the highest PET which is 9 times higher than that of conventional ligand capped PNCs. These results highlight the impact of surface chemistry on the excited-state interactions of $CsPbBr_3$ NCs and in photocatalytic applications. More importantly, this work concludes that amine-free PNCs maintain a redox-active surface with a high photoinduced electron transfer rate which makes them an ideal candidate for photocatalytic applications.

Introduction

Inorganic cesium lead halide perovskite nanocrystals ($CsPbX_3$, X = I, Br, Cl) have been of great interest to researchers because of their very high photoluminescence quantum yield (~up to 90%), broad absorbance, and narrow emission with wide spectral tunability.[1–7] These materials are at the forefront of research due to their low-temperature facile synthesis, tolerance to surface defects, and low exciton binding energies.[1,8–10] Due to these excellent optoelectronic properties[1,11–14] and facile synthesis PNCs received great attention as active materials in several optoelectronic devices such as light-emitting diodes,[15,16] solar cells,[17] photodetectors,[18] scintillators,[19] and photocatalysts.[20–22] The carrier diffusion in cesium lead halide perovskite PNCs plays an important role in the performance of optoelectronic devices.[23] Carrier diffusion is affected by several factors such as the energy levels, crystallinity, exciton binding energy, and surface chemistry of PNCs.[24–26] Typically, in optoelectronic devices upon photoexcitation, the exciton dissociates and the electron/hole is transferred from the conduction/valence band to the electron/hole acceptors, respectively.[27]

Hence examining the factors that impact the charge transport is significant for improving the performance of inorganic halide PNCs and broadening their applications. While most of these PNCs are used in photovoltaic[28] and optoelectronic devices,[29–32] only limited research has been done towards their use as photocatalysts.[33–35] The reason behind the limited use of PNCs in photocatalytic studies is their instability in the polar medium and the presence of high energy barrier surfactants on the surfaces of the nanocrystals. The use of surfactant molecules in PNC synthesis is unavoidable but it limits the access of the active surface sites to electron/hole acceptors.

The use of PNCs as photocatalysts was first realized by Park *et al.* when they reported their pioneering work using methylammonium lead iodide for hydrogen evolution from a saturated HI solution.[36] Soon after the initial work, many research groups reported photocatalytic applications which include CO_2 reduction,[37,38] derivatives of thiophene by polymerization,[33] oxidation of benzyl alcohol,[39] activation of $C(sp^3)$–H,[40] and alkylation of aldehydes.[41] Composite structures (such as $CsPbBr_3$ NCs with graphene oxide and with porous g-C_3N_4) have been utilized to enhance the charge transport efficiency for further improvement in photocatalytic conversion.[36,37] Thus the use of secondary conducting materials as co-catalysts has been proved as a successful strategy. Nevertheless, direct modification of PNCs may be the most viable and straightforward option to accelerate charge transport which therefore improves the photocatalytic performance efficiency.[42]

To design an efficient photo-catalyst the competition between radiative charge recombination and charge transfer remains the main focus. In metal chalcogenide semiconductor

Department of Chemistry, SRM University-AP, Amaravati, Neerukonda, Guntur (Dt), Andhra Pradesh, 522240, India. E-mail: nimai.m@srmap.edu.in

† Electronic supplementary information (ESI) available. See DOI: 10.1039/d1na00091h

nanocrystals, efficient charge separation was achieved through morphological and band engineering modifications *via* core/shell heterostructures.[43,44] Band engineering with core/shell structures for efficient charge separation in perovskite nanocrystals is not yet well established. Hence, researchers are working on alternative techniques to improve interfacial charge separation. Modification in surface chemistry could be a viable option to improve charge separation and electron transfer.[45] Surface capping groups are necessary to improve their colloidal stability and maintain their morphology but their presence may reduce or even block interfacial carrier transfer. To overcome this problem, it is desirable to find out suitable surface capping ligands that can facilitate electron transfer while preserving the morphology and maintaining the stability of the perovskite NCs. Therefore, there is an urgent need for alternative surface capping groups that may facilitate faster charge transfer from PNCs to the acceptor.

Herein, we sought to investigate the effects of a new surface capping shell on the redox activity of PNCs. $CsPbBr_3$ PNCs with three different surface capping groups were synthesized and utilized as photoinduced electron donors. To understand surface capping shell-dependent charge transfer we performed photoinduced electron transfer (PET) experiments with a standard electron acceptor, benzoquinone (BQ). The schematic reaction mechanism is shown in Fig. 1. Previous studies have shown that a rapid PET occurs at the $CsPbBr_3$/BQ interface.[46] The PET process relies on the reduction potential of NCs and the permeability of the surface capping shell. The PET process has been probed with the help of steady-state and time-resolved PL of $CsPbBr_3$ PNCs with different concentrations of BQ molecules. The steady-state PL demonstrated an improved photoinduced electron transfer (PET) when completely amine-free $CsPbBr_3$ PNCs are used as photoactive materials. This could be attributed to the absence of the strongly binding oleylamine which facilitates the fast charge transfer process. This observation was further confirmed by the time-resolved photoluminescence spectra, in which the amine-free $CsPbBr_3$ NCs have the longest lifetime, therefore, this indicates longer existence of the exciton which can be easily dissociated and transferred to the electron acceptor. Thus, we envisioned that amine-free $CsPbBr_3$ PNCs could be an ideal candidate for a photocatalyst, and it will open a new avenue in PNC photocatalytic-based organic synthesis.

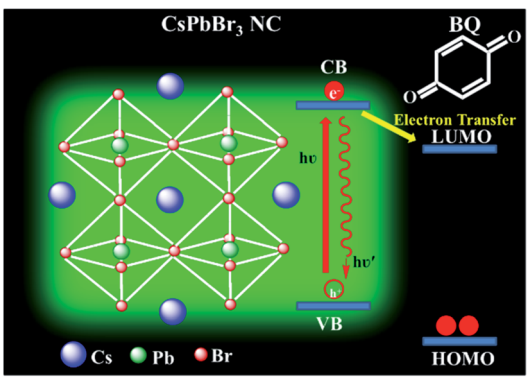

Fig. 1 Schematic energy level diagram of $CsPbBr_3$ NCs and the possible electron transfer that occurs from NCs to benzoquinone (BQ) molecule.

Results and discussion

Three different surface chemistry-based $CsPbBr_3$ perovskites were synthesized according to the reported hot injection method with a slight modification.[47,48] Briefly, amine free-$CsPbBr_3$ perovskite nanocrystals were prepared by a modified three-precursor approach in which the Cs, Pb, and Br precursors are used independently. Amine free-$CsPbBr_3$ PNCs were synthesized in the presence of oleic acid (OA) and trioctylphosphine (TOP) as surface capping ligands. In this process, oleylamine is replaced with TOP.

In contrast, amine-$CsPbBr_3$ PNCs were synthesized by the conventional two precursor approach where oleylamine (OAm) and oleic acid (OA) were used as surface capping ligands.[48] The amine + TOP capped $CsPbBr_3$ PNCs were synthesized by the above-mentioned conventional synthesis in the presence of TOP as the surface capping ligand in addition to OAm and OA. The detailed synthesis can be found in the Experimental section in the ESI.†

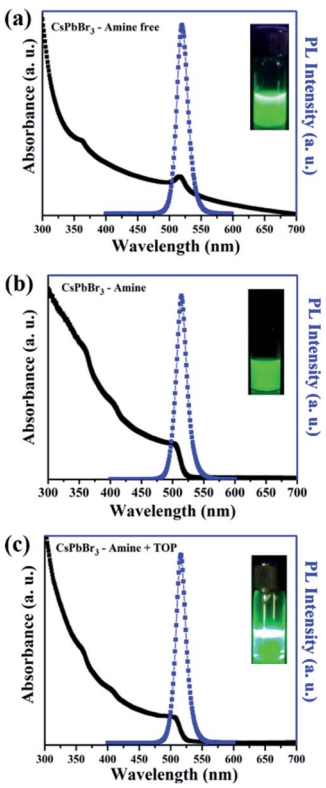

Fig. 2 UV-visible absorption (black line) and PL emission spectra (blue line) of as-synthesized $CsPbBr_3$ NCs (a) amine free (b) amine and (c) amine + TOP. The inset shows the images of the colloidal solution of NCs dispersed in toluene under UV light irradiation with excitation wavelength at 365 nm.

The detailed optical characterization of the three different surface ligand capped $CsPbBr_3$ PNCs can be found in Fig. 2. Fig. 2(a)–(c) show the narrow excitonic-emission spectra (blue color) and broad absorbance spectra (black line) of amine-free, amine, and amine + TOP based $CsPbBr_3$ PNCs and in the inset, the digital photograph of the colloidal solution taken under UV irradiation (with excitation wavelength of 365 nm) is provided, which shows good dispersibility in toluene and is highly emissive in nature. The calculated photoluminescence quantum yield (PLQY) values of the three samples are 69.2% (amine-free), 79.4% (amine), and 81.1% (amine + TOP). The absorbance and emission spectra with the 1st excitonic peak at 516 nm and the emission maximum at 518 nm are presented in Fig. 2(a) for amine-free $CsPbBr_3$ PNCs. The full width at half maximum (FWHM) of 23.4 nm indicates moderately monodisperse particles. The $CsPbBr_3$-amine PNCs and $CsPbBr_3$-amine + TOP PNCs exhibit absorption peaks at 510 nm and 511 nm and PL emission peaks at 513 nm (FWHM = 18.3 nm) and 517 nm (FWHM = 19.7 nm) respectively.

FTIR spectroscopy was used to characterize the surface chemistry of the three PNCs and to understand the surface–ligand interactions of surfactants (Fig. 3). For the amine-free and amine + TOP surface capped PNCs a peak around 1140 cm^{-1} is observed which is attributed to the P=O stretching vibration.[46] The spectra show the characteristic CH_2 stretching vibration at 2924 and bending vibration at 2854 cm^{-1}, and NH_2 bending vibration at 1636 cm^{-1}, together with the C=O stretching vibration at 1715 cm^{-1}. In the case of the amine-free synthesis, the presence of TOP along with $Pb(OA)_2$ may initiate the formation of TOPO by reaction with the carboxyl group of $Pb(OA)_2$, which is proposed owing to the peak at 1140 cm^{-1} that could be attributed to the P=O stretching vibration. Compared with the spectrum of pure TOPO, the shift in the absorption peak of P=O stretching from 1156 to 1140 cm^{-1} is attributed to bonding on the NC surface. The deformation bands at 1400–1440 cm^{-1} may be due to the presence of C–P interaction.[46]

From the FTIR analysis, we may presume the presence of the respective surface ligands on the three different PNCs, but to get an actual insight into the surface chemistry we may require further detailed characterization.

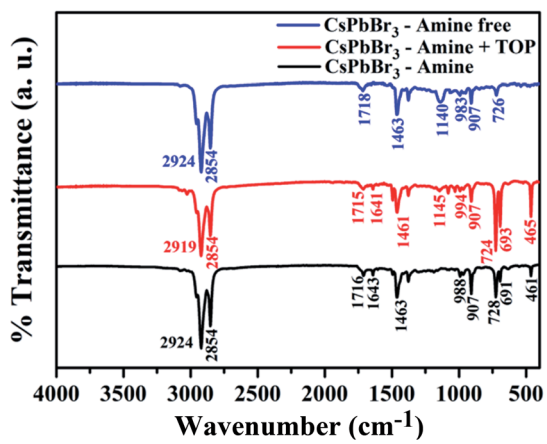

Fig. 3 FTIR spectra of $CsPbBr_3$ perovskite NCs synthesized using the three different surface capping groups.

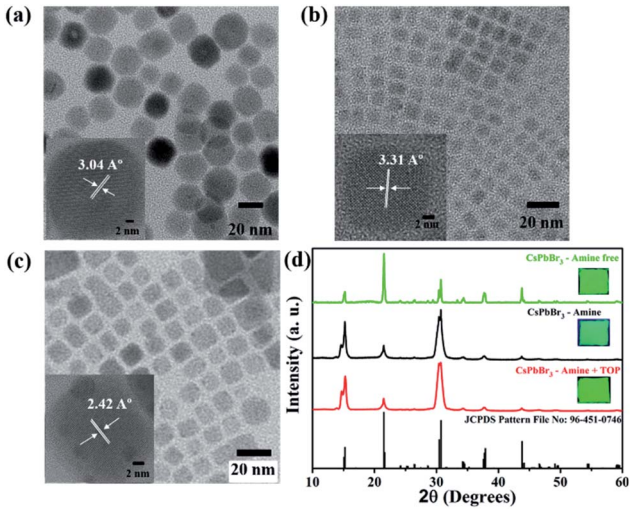

Fig. 4 TEM images and (inset) HRTEM images of as-synthesized $CsPbBr_3$ NCs: (a) amine-free, (b) amine, (c) amine + TOP and (d) XRD pattern of the three as-synthesized $CsPbBr_3$ NCs with the JCPDS pattern file. Inset shows the digital images of the corresponding films under UV light irradiation with excitation wavelength at 365 nm.

Transmission electron microscopy (TEM) was used to assess the structural properties of all the three $CsPbBr_3$ PNCs and showed good dispersity and uniform size distribution (Fig. 4(a)–(c)). The TEM images further confirmed that there is no aggregation. Insets of Fig. 4(a)–(c) show high-resolution transmission electron microscopy images of a single nanocrystal with a scale bar of 2 nm, which show the presence of defined lattice fringes indicating the high crystallinity of the nanocrystals. The lattice spacing of amine-free, amine and amine + TOP capped $CsPbBr_3$ NCs are 3.04, 3.31, and 2.42 Å, which correspond to the (121), (022) and (240) planes of the orthorhombic phase, respectively. The TEM image of the amine-free PNCs in Fig. 4(a) shows that the NCs have cubic morphology with an average particle size of 21.34 ± 2.8 nm. Fig. 4(b) and (c) present the transmission electron microscopy (TEM) images of the $CsPbBr_3$ sample with amine capped and amine + TOP capped NCs. The as-synthesized $CsPbBr_3$ NCs are cubic in shape and with varying surface ligands; the particle's morphology is largely maintained. In the case of amine and amine + TOP surfaces, the ligand capped $CsPbBr_3$ PNCs have good colloidal stability with moderate monodispersity (the calculated average particle sizes of the samples are 8.53 ± 1.3 nm and 12.72 ± 2.1 nm respectively).

X-ray diffraction patterns of all three $CsPbBr_3$ films made of the three different surface group capped NCs are shown in Fig. 4(d). The X-ray diffraction patterns confirmed that the PNCs are highly crystalline with the orthorhombic phase which is in good match with the JCPDS pattern file: 96-451-0746. The NC films were prepared by drop-casting the colloidal solutions of $CsPbBr_3$ NCs on a cleaned glass substrate and their respective photographs were taken under UV light irradiation with excitation wavelength at 365 nm.

Due to their large extinction coefficient in the visible range ($\sim 10^6$ M^{-1} cm^{-1})[46,49] and low exciton binding, cesium lead halide ($CsPbX_3$) PNCs provide an excellent opportunity for light absorption and subsequent photoinduced charge separation. Because of low electron and hole trapping which is typical of PNCs, facile electron and hole transfer has been observed in unmodified nanocrystals. A variety of organic syntheses have been demonstrated with $CsPbBr_3$ NCs as efficient photoredox catalysts.[41,49] But the presence of long-chain surface capping groups affects the charge transfer from $CsPbBr_3$ NCs to the electron/hole acceptor. The surface ligand shell plays a critical role in stabilizing the crystalline phase of halide perovskite NCs. Due to their more ionic nature, these materials often suffer from phase transformation or dissolution.[50] Moreover, we overcome the problem of charge separation and stability in PNCs by a simple and controllable method that involves the judicious choice of suitable surface capping groups. Here we have investigated different surface ligand capped PNCs to study their photo redox activity and performed a photoinduced electron transfer (PET) experiment with the standard electron acceptor, benzoquinone (BQ) molecule.

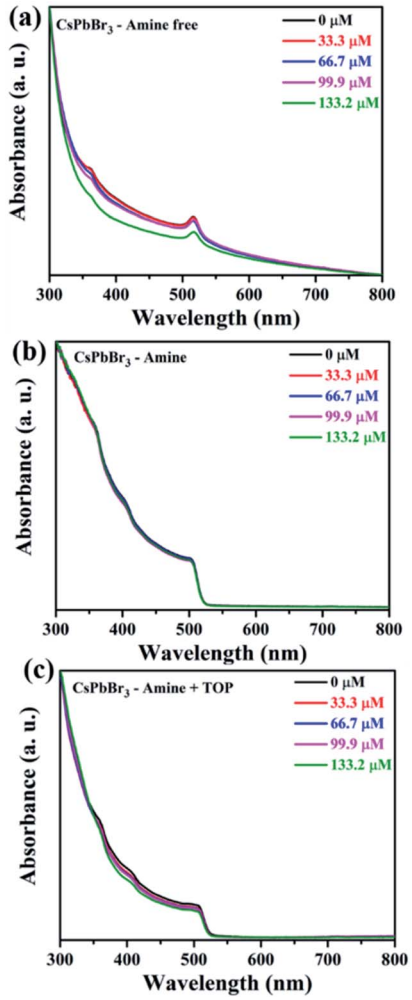

Fig. 5 Absorption spectra of $CsPbBr_3$ PNCs with the incremental addition of BQ: (a) amine-free (b) amine capped and (c) amine + TOP capped PNCs. All the samples for optical measurements are prepared in toluene solution.

Firstly, we investigated the influence of benzoquinone addition on the absorption spectra of $CsPbBr_3$ nanocrystals capped with the three different ligand systems. Toluene is used as a solvent for the dispersion of both nanocrystals and benzoquinone. The concentration of all three PNC samples was determined from absorption spectroscopy using the reported extinction coefficients.[51] Fig. 5(a)–(c) show the absorption spectra of $CsPbBr_3$ prepared with OA/TOP (amine-free), OA/OAm ligands, and OA/OAm/TOP ligands. The benzoquinone was added incrementally to each PNC solution (same concentration of PNCs) and the absorption spectra were recorded at several concentrations.

The amine-free $CsPbBr_3$ PNCs with OA/TOP ligands showed a large degree of scattering and upon addition of BQ, there is not much change observed (Fig. 5(a)). The dynamic nature of surface capping ligands hinders their complete dispersion and thus gives rise to a scattering effect. On the other hand, for the amine and amine + TOP capped $CsPbBr_3$ PNCs there was no scattering (Fig. 5(b) and (c)) with no obvious changes in absorption upon sequential addition of BQ. The absence of scattering of these two PNCs is due to oleylamine, the presence of which results in good dispersion of the NCs in solution. Fig. 6(a)–(c) show the photoluminescence (PL) spectra of the nanocrystals with OA/TOP (amine-free), OA/OAm ligands, and OA/OAm/TOP ligands, respectively with the stepwise addition of benzoquinone. In each case, the PL of $CsPbBr_3$ PNCs is quenched upon the addition of benzoquinone. On the top panel of Fig. 6, the change in PL intensity can be seen from the cuvettes (without and with BQ) under UV light irradiation. We analysed the fluorescence quenching data by considering the equilibrium between benzoquinone and $CsPbBr_3$ (reaction (1)).

$$BQ + CsPbBr_3 \overset{K_{app}}{\rightleftharpoons} [BQ - CsPbBr_3] \quad (1)$$

The binding interaction between BQ and $CsPbBr_3$ PNCs was studied using the double reciprocal plot following the Benesi–Hildebrand equation.[52] K_{app} in the above equation is the apparent association constant between BQ and $CsPbBr_3$ PNCs. Using the double reciprocal plot of the emission quenching data, K_{app} is evaluated. We found that OA/TOP (amine-free), OA/OAm (amine) ligands, and OA/OAm/TOP (amine + TOP) ligand capped PNCs have an association constant K_{app} of $\sim 5.3 \times 10^3$, $\sim 4.6 \times 10^3$ M^{-1}, and $\sim 7.5 \times 10^3$ M^{-1} respectively. The apparent association constant (K_{app}) values for three different surface chemistry based PNCs with benzoquinone molecule are in the same order. The similar K_{app} values indicate a relatively similar binding between nanocrystals and BQ molecules for all the three PNC samples. Despite the long capping ligands of all the three $CsPbBr_3$ PNCs, their surface is still accessible for interaction with redox-active molecules. The photoluminescence (PL) decay using time-correlated single-photon counting (TCSPC) has been used to probe the effect of BQ on the radiative excited state of $CsPbBr_3$. Fig. 7 shows the decay of the photoluminescence monitored at the emission maximum for PNCs

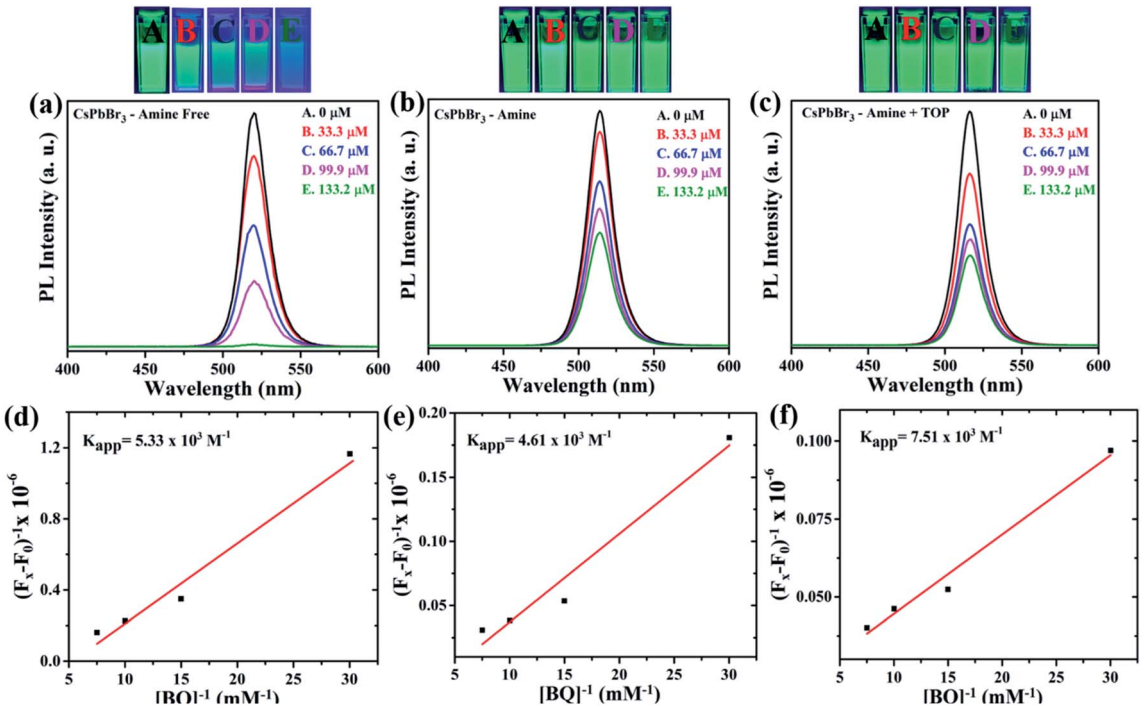

Fig. 6 Steady state PL of as-synthesized $CsPbBr_3$ NCs with different surface ligands with various concentrations of BQ molecule (0–133.2 μM) (a) amine-free (b) amine and (c) amine + TOP. Pictures under UV light with excitation wavelength at 365 nm above the graphs with labelling (A–E, with different concentrations of BQ molecule). (d–f) Double reciprocal analysis of the fluorescence quenching data, and the apparent association constants (K_{app}). All spectra were recorded in toluene solvent.

with the three different surface chemistries. The native PL lifetime (*i.e.*, without BQ) is the highest for amine-free OA/TOP-capped $CsPbBr_3$ ($\bar{\tau}_{avg} \sim 17.03$ ns). For amine and amine + TOP capped $CsPbBr_3$, the native lifetime is lower. In each case, sequential addition of BQ decreases the PL lifetime which indicates electron transfer from the excited $CsPbBr_3$ to the surface-bound BQ. In the case of amine-free PNCs, the rapid quenching of the $CsPbBr_3$ excited state by BQ indicates that a fast electron transfer process dominates (eqn (2)). Furthermore, the photo-induced electron transfer (PET) process is quantitatively analyzed with the help of time-resolved PL and steady-state PL of the $CsPbBr_3$ NCs with various concentrations of BQ molecules. The PET process depends on the reduction potential of the $CsPbBr_3$ NCs and the permeability of the surface binding ligands.[53] As shown in Fig. 6(a) and 7(a), the PL and TCSPC spectra of amine-free $CsPbBr_3$ NCs, we find that the PL properties of these PNCs are dynamically quenched by BQ when compared to amine-$CsPbBr_3$ NCs and amine + TOP-$CsPbBr_3$ NCs as shown in Fig. 6(b), 7(b) and 6(c), 7(c) respectively. The Stern–Volmer equation has been used to study the charge transfer process (eqn (3)) as shown in Fig. 8.

Table 1 Key parameters of photoinduced electron transfer from $CsPbBr_3$ NCs to benzoquinone (BQ) molecules

$CsPbBr_3$ NCs	K_{SV} (mM^{-1})	$\bar{\tau}_0$ (ns)	K_q (M^{-1} ns^{-1})	K_q improvement
Amine-free	106.79	17.03	6270	8.8
Amine + TOP	36.33	11.68	3110	2.01
Amine	7.34	10.30	712	1

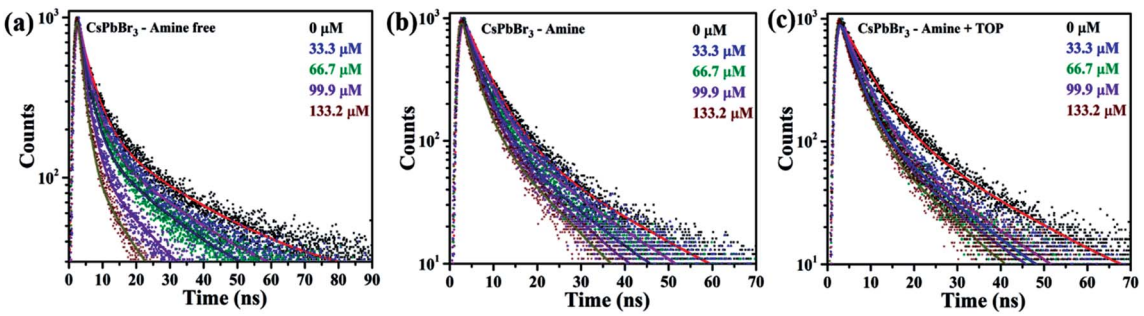

Fig. 7 Time-resolved PL spectra, the solid lines are the fit with the bi-exponential function: (a) amine-free (b) amine and (c) amine + TOP (λ_{ex} = 370 nm).

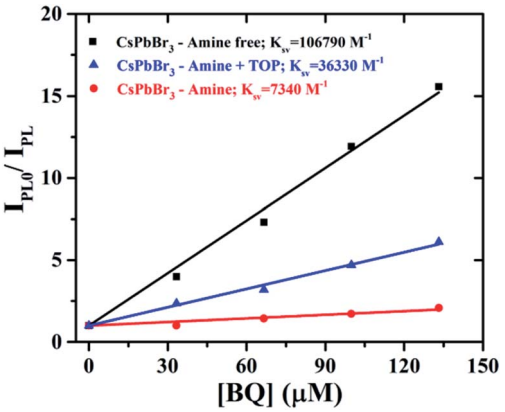

Fig. 8 I_{PL0}/I_{PL} *vs.* [BQ] of $CsPbBr_3$ NCs with different surface ligands (black: amine-free, blue: amine, and red: amine + TOP). I_{PL0} represents the steady-state PL intensity of $CsPbBr_3$ without BQ molecule; I_{PL} represents the steady-state PL intensity of $CsPbBr_3$ with different concentrations of BQ molecule.

$$[CsPbBr_3\text{–}BQ] + h\nu \rightarrow [CsPbBr_3(h\text{–}e)\text{–}BQ] \rightarrow [CsPbBr_3(h)\text{–}BQ^{\bullet}] \quad (2)$$

$$I_{PL0}/I_{PL} = 1 + K_{SV}[BQ] = 1 + K_q\bar{\tau}_0[BQ]. \quad (3)$$

where K_{SV} is the steady-state Stern–Volmer quenching constant, I_{PL0} and I_{PL} are the PL intensity without BQ and PL intensity with various concentrations of BQ. Furthermore, the linear relationship between I_{PL0}/I_{PL} and the concentration of BQ, [BQ], implies that the PET process is diffusion-limited.[45] The bimolecular quenching constant, K_q, can be obtained using the steady-state Stern–Volmer quenching constant (K_{SV}) and average lifetime from eqn (3). $\bar{\tau}_0$ is the intensity-average lifetime constant from the bi-exponential fit to the $CPbBr_3$ NCs without any electron acceptor. All the quenching constants are mentioned in Table 1. Amine-free PNCs have the highest K_{SV} when compared to the conventional amine-based and amine + TOP capped $CsPbBr_3$ NCs. The bimolecular quenching constant K_q, of amine-free PNCs, is nearly 8.8 times higher when compared to the amine-$CsPbBr_3$ NCs. The larger K_{SV} value for amine-free $CsPbBr_3$ NCs is due to their enhanced ligand permeability which impacts their redox potential. Thus, we can hypothesize that surface chemistry plays a vital role in enhancing the charge separation but further studies are needed to understand the effect of various other factors.

Conclusions

In summary, we investigated the impact of the surface chemistry of $CsPbBr_3$ PNCs on the excited state interactions and interfacial charge transfer to a redox molecule. We compared the charge transfer process with $CsPbBr_3$ PNCs synthesized with OA/OAm, OA/TOP (amine-free), and OA/OAm/TOP as surface capping ligands. The surface chemistry based binding interaction between the electron acceptor (BQ) and $CsPbBr_3$ PNCs was studied. All three ligands based $CsPbBr_3$ PNC system exhibits a similar apparent association constant. More interestingly, we found that the surface chemistry has a substantial influence on charge transfer efficiency. The amine-free $CsPbBr_3$ PNCs (OA + TOP as ligands) exhibited the highest photoinduced electron transfer (PET) efficiency which was 9 times higher than that of the conventional amine/oleic acid-based $CsPbBr_3$ system. Our work highlights that through controlling the surface ligand shells we can tune the photoredox activity of $CsPbBr_3$ PNCs. Thus, we envisioned that this work will provide new insights for the future design of halide perovskite nanomaterials suitable for photocatalytic reactions.

Author contributions

S. A. conducted all syntheses, under the guidance of N. M. S. A. and V. G. V. D. analysed the optical spectroscopy data under the guidance of N. M. S. A. and N. M. wrote the manuscript.

Conflicts of interest

There are no conflicts to declare.

Acknowledgements

We acknowledge the HRTEM FACILITY at the SRMIST set up with support from MNRE (Project no. 31/03/2014-15/PVSER&D), Government of India.

References

1 L. Protesescu, S. Yakunin, M. I. Bodnarchuk, F. Krieg, R. Caputo, C. H. Hendon, R. X. Yang, A. Walsh and M. V. Kovalenko, *Nano Lett.*, 2015, **15**, 3692–3696.
2 G. Almeida, O. J. Ashton, L. Goldoni, D. Maggioni, U. Petralanda, N. Mishra, Q. A. Akkerman, I. Infante, H. J. Snaith and L. Manna, *J. Am. Chem. Soc.*, 2018, **140**, 14878–14886.
3 M. Li, X. Zhang, Y. Du and P. Yang, *J. Lumin.*, 2017, **190**, 397–402.
4 M. Li, X. Zhang, T. Dong, P. Wang, K. Matras-Postolek and P. Yang, *J. Phys. Chem. C*, 2018, **122**, 28968–28976.
5 A. Swarnkar, R. Chulliyil, V. K. Ravi, M. Irfanullah, A. Chowdhury and A. Nag, *Angew. Chem.*, 2015, **127**, 15644–15648.
6 V. G. V. Dutt, S. Akhil and N. Mishra, *ChemNanoMat*, 2020, **6**, 1730–1742.
7 S. Akhil, V. G. V. Dutt and N. Mishra, *ChemNanoMat*, DOI: 10.1002/cnma.202100002.
8 B. A. Koscher, J. K. Swabeck, N. D. Bronstein and A. P. Alivisatos, *J. Am. Chem. Soc.*, 2017, **139**, 6566–6569.
9 F. Di Stasio, S. Christodoulou, N. Huo and G. Konstantatos, *Chem. Mater.*, 2017, **29**, 7663–7667.
10 H. Lin, C. Zhou, Y. Tian, T. Siegrist and B. Ma, *ACS Energy Lett.*, 2018, **3**, 54–62.
11 M. V. Kovalenko, L. Protesescu and M. I. Bodnarchuk, *Science*, 2017, **358**, 745–750.
12 S. Bai, Z. Yuan and F. Gao, *J. Mater. Chem. C*, 2016, **4**, 3898–3904.

13 G. Rainò, G. Nedelcu, L. Protesescu, M. I. Bodnarchuk, M. V. Kovalenko, R. F. Mahrt and T. Stöferle, *ACS Nano*, 2016, **10**, 2485–2490.
14 K. Chen, S. Schünemann, S. Song and H. Tüysüz, *Chem. Soc. Rev.*, 2018, **47**, 7045–7077.
15 E. Yassitepe, Z. Yang, O. Voznyy, Y. Kim, G. Walters, J. A. Castañeda, P. Kanjanaboos, M. Yuan, X. Gong, F. Fan, J. Pan, S. Hoogland, R. Comin, O. M. Bakr, L. A. Padilha, A. F. Nogueira and E. H. Sargent, *Adv. Funct. Mater.*, 2016, **26**, 8757–8763.
16 M. Meyns, M. Perálvarez, A. Heuer-Jungemann, W. Hertog, M. Ibáñez, R. Nafria, A. Genç, J. Arbiol, M. V. Kovalenko, J. Carreras, A. Cabot and A. G. Kanaras, *ACS Appl. Mater. Interfaces*, 2016, **8**, 19579–19586.
17 Q. A. Akkerman, M. Gandini, F. Di Stasio, P. Rastogi, F. Palazon, G. Bertoni, J. M. Ball, M. Prato, A. Petrozza and L. Manna, *Nat. Energy*, 2016, **2**, 1–7.
18 P. Ramasamy, D.-H. Lim, B. Kim, S.-H. Lee, M.-S. Lee and J.-S. Lee, *Chem. Commun.*, 2016, **52**, 2067–2070.
19 Q. Chen, J. Wu, X. Ou, B. Huang, J. Almutlaq, A. A. Zhumekenov, X. Guan, S. Han, L. Liang, Z. Yi, J. Li, X. Xie, Y. Wang, Y. Li, D. Fan, D. B. L. Teh, A. H. All, O. F. Mohammed, O. M. Bakr, T. Wu, M. Bettinelli, H. Yang, W. Huang and X. Liu, *Nature*, 2018, **561**, 88–93.
20 Z.-C. Kong, J.-F. Liao, Y.-J. Dong, Y.-F. Xu, H.-Y. Chen, D.-B. Kuang and C.-Y. Su, *ACS Energy Lett.*, 2018, **3**, 2656–2662.
21 J. Hou, S. Cao, Y. Wu, Z. Gao, F. Liang, Y. Sun, Z. Lin and L. Sun, *Chem.–Eur. J.*, 2017, **23**, 9481–9485.
22 G. Gao, Q. Xi, H. Zhou, Y. Zhao, C. Wu, L. Wang, P. Guo and J. Xu, *Nanoscale*, 2017, **9**, 12032–12038.
23 C. S. Ponseca, E. M. Hutter, P. Piatkowski, B. Cohen, T. Pascher, A. Douhal, A. Yartsev, V. Sundström and T. J. Savenije, *J. Am. Chem. Soc.*, 2015, **137**, 16043–16048.
24 A. Giampietri, G. Drera and L. Sangaletti, *Adv. Mater. Interfaces*, 2017, **4**, 1700144.
25 C. de Weerd, L. Gomez, H. Zhang, W. J. Buma, G. Nedelcu, M. V. Kovalenko and T. Gregorkiewicz, *J. Phys. Chem. C*, 2016, **120**, 13310–13315.
26 K. Zheng, Q. Zhu, M. Abdellah, M. E. Messing, W. Zhang, A. Generalov, Y. Niu, L. Ribaud, S. E. Canton and T. Pullerits, *J. Phys. Chem. Lett.*, 2015, **6**, 2969–2975.
27 Q. Hu, E. Rezaee, Q. Dong, H. Shan, Q. Chen, L. Wang, B. Liu, J.-H. Pan and Z.-X. Xu, *Sol. RRL*, 2019, **3**, 1800264.
28 M. Kulbak, D. Cahen and G. Hodes, *J. Phys. Chem. Lett.*, 2015, **6**, 2452–2456.
29 J. B. Hoffman, G. Zaiats, I. Wappes and P. V. Kamat, *Chem. Mater.*, 2017, **29**, 9767–9774.
30 E. M. Sanehira, A. R. Marshall, J. A. Christians, S. P. Harvey, P. N. Ciesielski, L. M. Wheeler, P. Schulz, L. Y. Lin, M. C. Beard and J. M. Luther, *Sci. Adv.*, 2017, **3**, eaao4204.
31 Y. Hu, F. Bai, X. Liu, Q. Ji, X. Miao, T. Qiu and S. Zhang, *ACS Energy Lett.*, 2017, **2**, 2219–2227.
32 S. Xiang, Z. Fu, W. Li, Y. Wei, J. Liu, H. Liu, L. Zhu, R. Zhang and H. Chen, *ACS Energy Lett.*, 2018, **3**, 1824–1831.
33 K. Chen, X. Deng, G. Dodekatos and H. Tüysüz, *J. Am. Chem. Soc.*, 2017, **139**, 12267–12273.
34 H. Lu, X. Chen, J. E. Anthony, J. C. Johnson and M. C. Beard, *J. Am. Chem. Soc.*, 2019, **141**, 4919–4927.
35 X. Luo, R. Lai, Y. Li, Y. Han, G. Liang, X. Liu, T. Ding, J. Wang and K. Wu, *J. Am. Chem. Soc.*, 2019, **141**, 4186–4190.
36 S. Park, W. J. Chang, C. W. Lee, S. Park, H.-Y. Ahn and K. T. Nam, *Nat. Energy*, 2016, **2**, 1–8.
37 Y.-F. Xu, M.-Z. Yang, B.-X. Chen, X.-D. Wang, H.-Y. Chen, D.-B. Kuang and C.-Y. Su, *J. Am. Chem. Soc.*, 2017, **139**, 5660–5663.
38 M. Ou, W. Tu, S. Yin, W. Xing, S. Wu, H. Wang, S. Wan, Q. Zhong and R. Xu, *Angew. Chem.*, 2018, **130**, 13758–13762.
39 S. Schünemann, M. van Gastel and H. Tüysüz, *ChemSusChem*, 2018, **11**, 2057–2061.
40 H. Huang, H. Yuan, J. Zhao, G. Solís-Fernández, C. Zhou, J. W. Seo, J. Hendrix, E. Debroye, J. A. Steele, J. Hofkens, J. Long and M. B. J. Roeffaers, *ACS Energy Lett*, 2019, **4**, 203–208.
41 X. Zhu, Y. Lin, Y. Sun, M. C. Beard and Y. Yan, *J. Am. Chem. Soc.*, 2019, **141**, 733–738.
42 Y. Li, Q. Shu, Q. Du, Y. Dai, S. Zhao, J. Zhang, L. Li and K. Chen, *ACS Appl. Mater. Interfaces*, 2020, **12**, 451–460.
43 S. W. Tong, N. Mishra, C. L. Su, V. Nalla, W. Wu, W. Ji, J. Zhang, Y. Chan and K. P. Loh, *Adv. Funct. Mater.*, 2014, **24**, 1904–1910.
44 N. Mishra, V. G. Vasavi Dutt and M. P. Arciniegas, *Chem. Mater.*, 2019, **31**, 9216–9242.
45 H. Lu, X. Zhu, C. Miller, J. San Martin, X. Chen, E. M. Miller, Y. Yan and M. C. Beard, *J. Chem. Phys.*, 2019, **151**, 204305.
46 K. Wu, G. Liang, Q. Shang, Y. Ren, D. Kong and T. Lian, *J. Am. Chem. Soc.*, 2015, **137**, 12792–12795.
47 S. Akhil, V. G. V. Dutt and N. Mishra, *Chem.–Eur. J.*, 2020, **26**, 17195–17202.
48 V. G. V. Dutt, S. Akhil and N. Mishra, *CrystEngComm*, 2020, **22**, 5022–5030.
49 X. Zhu, Y. Lin, J. San Martin, Y. Sun, D. Zhu and Y. Yan, *Nat. Commun.*, 2019, **10**, 2843.
50 J. Shamsi, A. S. Urban, M. Imran, L. De Trizio and L. Manna, *Chem. Rev.*, 2019, **119**, 3296–3348.
51 J. De Roo, M. Ibáñez, P. Geiregat, G. Nedelcu, W. Walravens, J. Maes, J. C. Martins, I. Van Driessche, M. V. Kovalenko and Z. Hens, *ACS Nano*, 2016, **10**, 2071–2081.
52 J. T. DuBose and P. V. Kamat, *J. Phys. Chem. C*, 2020, **124**, 12990–12998.
53 K. E. Knowles, M. Tagliazucchi, M. Malicki, N. K. Swenson and E. A. Weiss, *J. Phys. Chem. C*, 2013, **117**, 15849–15857.